Manuscript of the article:

Yaniv, R., Yair, Y. , Price, C., Bór, J., Sato, M., Hobara, Y., Cummer, S., Li, J., Devir, A.,

Ground-based observations of the relations between lightning charge-moment-change and the physical and optical properties of column sprites.

Appeared in:

Journal of Atmospheric and Solar-Terrestrial Physics, 2014, Volume 107, Pages 60-67

Publisher's version:

http://dx.doi.org/10.1016/j.jastp.2013.10.018

Ground-based observations of the relations between lightning charge-moment-change and the physical and optical properties of column sprites

Roy Yaniv[1], Yoav Yair[1], Colin Price[2], Jo'zsef B'or[3], Mitsutero Sato[4], Yasuhide Hobara[5]

Steve Cummer[6], Jingbo Li[7] and Adam Devir[8]

[1] The Open University, Ra'anana, Israel
[2] Tel-Aviv University, Tel-Aviv, Israel.
3 Geodetic Observatory, Sopron, Hungary
4 Hokkaido University, Sapporo, Japan
5University of Telecommunication, Tokyo, Japan
6 Duke University, Durham, NC, USA
7 Intel Corporation, Hillsboro, Oregon, USA
8 IARD - Sensing Solutions Ltd., Yagur, Israel

Submitted to JASTP

1.1.2013

Revised, August 2013

Corresponding author:
Prof. Yoav Yair
Department of Life and Natural Sciences
The Open University of Israel
1 University Road, Ra'anana 43107 Israel

E-mail: yoavyair@gmail.com and yoavya@openu.ac.il
office: +972-9-7781217 fax: +972-9-7780661
mobile: +972-52-5415091

Abstract:

Optical observations of 66 sprites, using a calibrated commercial CCD camera, were conducted in the 2009 – 2010 and 2010 - 2011 winter seasons as part of the ILAN (Imaging of Lightning And Nocturnal flashes) campaign in the vicinity of Israel and the eastern Mediterranean. We looked for correlations between the properties of the parent lightning (specifically, the charge moment change; CMC) to the properties of column sprites, such as the measured radiance, the length of column sprites and the number of column elements in each sprite event. The brightness of sprites positively correlates with the CMC (0.7) and so does the length of sprite elements (0.83). These results are in agreement with previous studies, and support the QE model of sprite generation.

1. Introduction

Sprites are one of the most familiar types of Transient Luminous Events (TLEs) which occur in the upper atmosphere above thunderstorms. They are spectacular and beautiful, exhibiting complex structures and shapes [Pasko et al., 2011; B'or et al., 2013]. Sprites are likely generated by the quasi electrostatic field (QSF) induced by a parent lightning flash, most often of positive polarity (+CG) [Pasko et al 2007]. During such discharges, large amount of positive charge is lowered to the ground, and the remaining charge of opposite sign above the thundercloud generates the QSF in atmospheric layers below the ionosphere, for a very short time periods ~1–50 ms. The Charge-Moment-Change (CMC) is a parameter of the parent lightning and is defined as the product of the charge and the height from which it was lowered [Pasko et al., 1997; Cummer et al., 2006]. The CMC threshold for sprite generation is varying and no single value can be considered as the

lower limit. Hu et al. [2002] found that the probability for parent flashes with CMC > 1000 C·km in less than 6 ms to generate sprites was above 90%, while it was below 10% for lightning with CMC < 600 C·km. In an "exceptional case" (to use their words) Hu et al. [2002] reported that a lightning flash with a CMC as low as 120 C·km was sufficient to generate sprites. Cummer and Lyons [2005] reported threshold values of 350 C·km, and 600 C·km on two different nights, reflecting the inter-night variability in mesospheric conductivity. The impulsive CMC (iCMC) is an empirical definition, referring to the amount of charge lowered within the first 2 ms of the onset lightning's return stroke multiplied by the original height above the ground from which it was lowered [Cummer and Lyons, 2005; Lu et al., 2012]. For short-delayed sprites (less than 5 ms), a 75% probability for the generation of sprites required an iCMC larger than 300 C·Km [Lyons et al., 2009]. The smaller values of CMC for sprite generation were explained recently with a numerical model by Qin et al. [2012]. They showed that sprites can be produced even by weak flashes with CMC values ~200 C km, provided that vertically elongated in-homogeneities in the electron density exist in the ionosphere at altitudes near 90 km. Adachi et al. [2004] studied the possible correlation between the properties of the parent lightning (e.g peak current and CMC) and the properties of column sprites (number of column elements and length of columns). They found correlation between the CMC values and the lengths of column sprites and between the peak current values to the number of column elements of a sprite event.

Strong +CGs that exceed a threshold CMC are frequently produced in summer-time mesoscale convective systems (MCSs) [Lyons 2009], and also by smaller winter-time thunderstorms, like those that are found west of Japan's coastline [Matsudo et al., 2007 ;

Suzuki et al., 2011] and in the Eastern Mediterranean [Ganot et al., 2007; Yair et al., 2009]. Winter thunderstorms are often characterized by small convective cells embedded in a large stratiform area, with a vertical scale of few km [Yair et al., 2009]. A typical synoptic situation is shown in Figure 1, where a cold front of a deep Cyprus Low is situated west of the Israeli coastline, such that a clear line of sight exists to the thunderstorm cells. Lightning locations are based on the WWLLN data for ranges outside the coverage of the Israeli Lightning Detection Network, which is operated by the Israeli Electrical Corporation. For such meteorological conditions, thunderstorms produce lightning with large CMC which should suffice for sprite generation. Similar conditions exist in winter over the Sea of Japan [Takahashi et al., 2003, . In Eastern Mediterranean winter thunderstorms CMC values for sprite generation were found to be in the range 600 – 2800 C Km [Greenberg et al., 2007]..

Ground-based calibrated optical observations to measure the radiance of sprites were first performed by the ILAN team from Israel in the winter of 2008-9 [Yaniv et al., 2009]. The calibration procedure of the cameras was similar to the one described by Yair et al. [2003] for the sprite observations conducted during the Mediterranean Israeli Dust Experiment (MEIDEX) on-board the space shuttle Columbia in January 2003. For accurate and reliable results they considered the extinction of light by absorption and scattering of the atmosphere (aerosols, water vapor, O_2) to obtain the attenuation of the radiance and the visibility. The procedure involved separating pixels illuminated by the sprite from pixels belonging to the background. This was done by averaging and subtracting the background pixels, and considering the sprite spectra, atmospheric

visibility and the transmittance of the atmosphere computed by the MODTRAN code. The total brightness of 5 different column sprites was found to range from 183-350 kR.

Recently, Takahashi et al. [2010] measured the CMC– sprite brightness relationship using the ISUAL/array photometer on board the FORMOSAT-2. The brightness was calculated for 14 events by measuring the photon flux of the $N_2$1PG and $N_2$2PG spectral bands, taking into account the background noise. Optical energies in [MJ] were found to be in the range 1.3 MJ – 58 kJ, with an average value of 300 kJ. The correlation coefficients between the parent flash CMC and sprite's luminosity were 0.93 for the $N_2$1PG and 0.91 for the $N_2$2PG, showing an excellent linear relationship, further supporting the QE model.

This work describes the newest results from ground-based observations of sprites employing the same calibration methodology as used by Yaniv et al. [2009], for 66 events recorded during winter campaigns conducted from Israel during 2009-2011.

2. Instruments and data

We used a standard commercial CCD camera– Watec 902H2 Ultimate operating with a frame rate of 33ms/frame, that is commonly used by other TLEs research groups in Europe and in Japan [Bor et al 2009, Soula et al., 2009]. The camera was fitted with a 12mm f/0.8 lens with a field of view (FOV) of 31^o(H) X 23^o(V). A special broadband filter (Archer Optx FLTR-BP720-25) was mounted on the camera. The spectral band of this filter (640-800nm) matches the first positive ($N_2$1P) emission of sprites (575-1187nm). The filter transmittance, the quantum efficiency of the camera, atmospheric transmittance and sprite spectrum [Hampton et al 1996] are shown in Figure 2. The

atmospheric transmittance was calculated using MODTRAN 4 code with mid-latitude winter atmospheric model for range from the point of observation on the ground to the sprite location of 400km assuming an altitude=80km (these are typical values of camera-sprite ranges for observations in the Eastern Mediterranean; Ganot et al., 2007] . The camera settings are described in detail in Yaniv et al. [2009].

3. Methodology

The camera was calibrated using a CI SR-20 black body with a 1.0" aperture and varying temperature between 50 ^{o}C and 1000^{o}C. In the calibration process a fixed gain and gamma setting of 0.45 were used. The radiance [ph/sec/str/cm^2] was calculated using Planck's law for temperature range of 400 - 510^{o}C without saturation. For each temperature setting a snapshot was taken using the *UFO-capture* program and was analyzed with the image processing software called ImageJ (see Fig. 2 in Yaniv et al., 2009). The calibration was performed for different temperatures in order to check if the calibration constant K' [GL/(ph/sec)] is a linear parameter or whether it shows a non-linear temperature (radiance) dependence. Figure 3 presents a non-linear cubic dependence of K' on the radiance of the source that is later factored into the analysis procedure.

a. Calibration with black-body

In the images, the mean GL of a pixel in the Region-of-Interest is defined as GLc and is expressed by Equation 1.

(1) $$GLc = GL_{offset} + K' \cdot IFOV \cdot A_{opt} \cdot \int \frac{P(\lambda, T_c)}{h\nu} \cdot \tau_c(\lambda, L_c) \cdot F(\lambda) \cdot QE(\lambda) \cdot d\lambda$$

Where K' is the calibration constant [GL/ph/sec], IFOV [str] is the instantaneous field of view of the camera pixel, A_{opt} [cm^2] is the clear aperture of the CCD lens, $P(\lambda,T_c)$ is the Planck's function [W/str/cm^2/μm] for wavelength λ and temperature T[K]. τ_c is the atmospheric transmittance calculated for calibration distance L_c=1m, F(λ) is the filter transmittance and QE is the quantum efficiency of the CCD. GL_{offset} is a residual GL value that is measured without any light present and is a small bias due to the dark current of the CCD.

The radiance is then calculated in similar manner to Eq. 1. Equation 2 expresses the measured GL (GL_m) value of a pixel illuminated by the sprite.

(2) $$GLm = GL_{offset} + K' \cdot IFOV \cdot A_{opt} \cdot \int \frac{N(\lambda)}{h\nu} \cdot \tau_m(\lambda, L_m) \cdot F(\lambda) \cdot QE(\lambda) \cdot d\lambda$$

We evaluate the sprite radiance N(λ) from GL_m using the calibration constant K' that we found in the calibration. τ_m is the measured transmittance for measured distance L_m obtained from MODTRAN code. The photon flux Fl_{pixel} (Eq. 3) is obtained by the method described earlier [Devir et al., 1997] assuming that we know that the spectral shape of N(λ) which is the spectrum of the sprite S(λ). Denoting $\Delta GL_m = GL_m - GL_{offset}$ we get:

(3) $$Fl_{pixel} = \int \frac{N(\lambda)\, d\lambda}{h\nu} = \frac{\Delta GL_m \cdot D_{ad}(L_m)}{K' \cdot IFOV \cdot A_{opt} \cdot \tau_{eq} \cdot \bar{R}}$$

Where D_{ad} is the factorization coefficient (Eq 4), τ_{eq} is the experimental system weighted atmospheric transmittance (Eq. 5) and R is the averaged system response (Eq. 6). Averaging Equation 3 over all the pixels whose GL value exceeds the upper limit of the background level (meaning they contain the combined sprite and background radiances) and subtracting the average radiance of the background (obtained from averaging equation 3 for those pixels whose GL was below the threshold), enables to isolate the radiance of the sprite.

(4) $$D_{ad}(L_m) = \frac{\int \tau_m(\lambda, L_m) \cdot F(\lambda) \cdot QE(\lambda) \cdot d\lambda \cdot \int S(\lambda) \cdot d\lambda}{\int S(\lambda) \cdot \tau_m(\lambda, L_m) \cdot F(\lambda) \cdot QE(\lambda) \cdot d\lambda \cdot \int d\lambda}$$

where:

(5) $$\tau_{eq} = \frac{\int \tau_m(\lambda, L_m) \cdot F(\lambda) \cdot QE(\lambda) \cdot d\lambda}{\int F(\lambda) \cdot QE(\lambda) \cdot d\lambda}$$

and:

(6) $$\bar{R} = \frac{\int F(\lambda) \cdot QE(\lambda) \cdot d\lambda}{\int d\lambda}$$

b. Calculation of sprite radiance

The radiance of column sprites, the lengths of individual column elements and number of elements were analyzed using several features of the ImageJ software. Calculation of the radiance of TLEs was made by two methods. The first method ("Event Frame" method) is based on using the video frame of the sprite event (Figure 4a, c and e). We measure the background area from the left and the right of the sprite, and an area that is a superposition of both background and sprite. The next step is to plot the number of pixels as a function of the GL of the three measured areas (Figure 5). The two histograms from left and right of the sprite show a similar structure although the left background appears to be slightly brighter. The values of the

background pixels range from 0 to 28, while the grey level values of the sprite pixels range from 0-69. We conclude that pixels with values smaller than 28 correspond to the background and pixels with values above 28 originate from the sprite and they contain the information on its radiance, combined with the background.

c. Video analysis

A common method for analyzing video images is to subtract two consecutive video frames. The camera produces interlaced video where each frame consists of two fields. In order to subtract frames, we used the "blend" option in the Virtual Dub software that was the video analysis tool. This subtraction helps to isolate the signal from the background, based on the assumption that it does not change significantly during this time-frame. We used the first frame as the one containing the sprite element, and the frame just before it. Subtracting the event frame from the non-event frame thus yields only the signal of the event, so calculations can be made for the pixels holding (in principle) only the TLE signal. Even though the time delay between subsequent frames is short (30 ms), background changes can still occur (for example, diffuse light from a distant lightning), and this is an error source for this method. The Subtracting Frames method is written as a MATLAB code that uses two successive video frames. The code subtracts the digital GL values in each pixel between both frames, thus isolating the pixels with the sprite signal. It then calculates the sprite radiance from the residual grey level. Figure 7 shows the “Subtracting-Frames” method.

We argue that the first method is more accurate since in the second method we risk calculating background pixels that might be light-contaminated by the sprite itself or

from other sprite elements in the area, and also by the scattered light from the parent flash. Again, scattered light from cloud tops can contaminate the area of the sprite erroneously, for example if the sprite appears low in the image, and will result with background pixels that are taken into consideration. Since the background is not uniform, minor changes can occur between the frames due to scattered city lights that change the grey level value of the pixels.

We cannot determine the sprite boundary due to the limited performance of the WATEC 902H2 camera, thus we may consider background pixels to be contaminated and illuminated by the sprite itself. Determining the sprite boundary is a hard task when using a low resolution camera (images size are 640 X 480, the camera is 8 bit – 256 colors). A good solution is to image sprites with high-speed cameras [Cummer et al., 2006; Montanya et al., 2010], but such an equipment was not available to us during these winter campaigns. To overcome the problem and find the boundaries on the right, left, bottom and the top of the sprite, we "sliced" the image with a horizontal cut (Figure 6) and vertical cut (Figure 8), by that we minimized the errors that might occur when using bare eye. Our method takes into consideration background pixels that are illuminated by the sprite event or by the lightning's scattered light and does not count them. This is done by repeating the procedure in each frame several times, by selecting different areas - first, an area that does not contain the sprite pixels (e.g. pixels that contain background pixels that are "pure" night and contaminated background pixels), and second, an area that contains the whole sprite event + background pixels.

d. Charge Moment Change

Charge moment change data were taken from 4 stations: in Nagicenk Geodetic Observatory in Sopron, Hungary, the Duke University station in North Carolina(USA), the Syowa station in Antarctica and the Moshiri, Hokkaido station in Japan. The common GPS time-base for all these systems enables the identification of signals that can be attributed to the parent flashes of the optically observed sprites, and the calculations of their respective CMCs. The number of events and respective CMCs are summarized in Table 1.

The Nagicenk Geodetic Observatory (NGC) in Sopron, Hungary, is described in detail by Satori et al. (2013). It has been monitoring the vertical electric field component in frequencies between 3 and 30 Hz using a very stable ball antenna. The horizontal magnetic field components have been regularly recorded using induction coils. The technique discussed by Huang et al. (1999) was used to estimate the location, polarity, and charge moment change of the parent lightning flashes from the Q-bursts found in the ELF data at NCK (Boccippio et al., 1999), as previously employed for TLEs detected during the MEIDEX (Price et al., 2004).

The ELF electromagnetic field has been continuously monitored in Moshiri (MSR) station, Hokkaido, Japan (44.2◦N, 142.2◦E) operated by the University of Electro-Communications since 1996 (Hobara et al., 2000, 2001). The Moshiri Observatory is considered to be one of the electromagnetically quietest places in Japan. Two horizontal magnetic fields are measured by orthogonally oriented induction search coils, aligned with geographical north and east, respectively. The vertical electric field is observed with a capacitor-type antenna. These antenna systems are fully calibrated and sampled at the frequency of 4000 Hz with a pass-band of 1 kHz, so that the

wave-forms of ELF signals (Schumann resonances, ELF transients, etc.) are continuously recorded for any further analysis. A GPS receiver provides an absolute time stamp for each sampling point. The CMC values for flashes detected at Moshiri were also calculated based on the impulsive estimation similar to the one in Huang et al. [1999].

The Syowa station in Antarctica (69.0°S, 39.6°E) capabilities and mode of operation are described in detail by Sato et al. (2003, see Figure 1 there). The ELF observation system consists of two search coil sensors in the range 1-100 Hz, located at West Ongul island, 5 km southeast of the Syowa station itself (in order to avoid man-made noise). The ELF data is amplified and then transmitted to the station by telemetry in the VHF band and are stored, together with the IRIG-E time stamp at 0.1 ms accuracy. After additional amplification the signals are sampled at 1000Hz. The computation algorithm of CMC values of the detected parent in Sato et al. [2008] is based on the principles described in Burke and Jones [1996].

The station at Duke University is described in detail in Hu et al. [2002]. It is monitoring ELF/VLF magnetic field data continuously at a field site near Duke University (35.975°N, −79.100°E), in the range 30 Hz-6 kHz. The sampling frequency of the data is 25 kHz and the GPS time insertion enables a sub-millisecond timing resolution.

For each sprite that was imaged in the Eastern Mediterranean, an ELF signal of the parent lightning was found by at least one station. Some showed a clear signal and enabled the calculation of a CMC value, but several events were ambiguous due to overlapping signals with several Q-bursts,. Such cases may lead to invalid estimations that made parent lightning assignment to the sprite unclear and the CMC value unreliable.

The reliability and stability of the values deduced this way is mirrored by the distribution of CMC values for the same sources by different methods and stations as presented in Williams et al. [2010]. By averaging the values obtained from several stations for the same parent flash, we obtained 10% accuracy of the CMC value, which may be considered a conservative estimate. In several cases the CMC values relied on values of two stations that detected the signal, while in others this was done by taking a single value of a single station.

e. Sprite morphology

The length of sprites can be calculated using two methods. The first method is best for situations when stars are visible in the background together with the TLEs. The image is then super-posed on a digital sky map software (for example: SkyCharts) to obtain an accurate azimuth and elevation [Ganot et al., 2007]. When stars are not visible in the image, we use the angular aperture of the camera, approximate distance to the parent lightning and the size of the image in pixels. The distance was derived from the camera location to the cluster of cloud-to-ground lightning flashes that occurred around the time of sprite detection. This usually defines an electrically active cell (Yair et al., 2009) with a size of several km. For an average range of 300-400 km from the shore, this leads to a marginal error in location, and hence to a small error in the calculation of sprite elevation and dimensions. To determine the length of the sprite in pixels we use a vertical-cut technique that generates a plot where we can determine the upper and lower boundaries of the sprite based on the values of the grey-level in the bright and dark pixels. This

enables counting the number of sprite-pixels that can be then converted to the length of the sprite. Figure 8 shows an example of such a vertical-cut through a sprite column.

A simple way to determine the number of elements in a sprite event is by visually counting the elements one by one. When it is suspected that there are weaker elements that are too dim or if elements overlap and hard to distinguish, we again use the horizontal cut technique (Figure 7). The peaks in the graph correspond to pixels with a higher GL value. These pixels represent the sprites that are seen in the upper part of Figure 6. The minimal values between the sprite elements represent the background pixels. From the detailed histogram we can clearly see which pixels belong to the sprite element, and thus deduce the number of elements.

4. Results and discussion

During the ILAN winter campaigns in the 2009-10 and 2010-11 seasons, a total of 66 sprites were imaged, in a quality that enabled analysis in the methods described in section 3. The sprite types were columns, carrots, jellyfishes and some undistinguished types. The brightness of each sprite event was evaluated at least three times using the first method (Event Frame), in order to obtain the average and mean error. The process was repeated by selecting different rectangles with varying pixel numbers that included background and sprite radiance and background only. The average mean error in the 3 re-calculations was 1% of the sprite's radiance. A comparison between the methods was done by measuring sample sprite events that were calculated with both methods. The average mean difference of the sprite's radiance obtained in the two methods is ~7%. The CMC values of the parent lightning, computed for 23 events, were found to range from

110 to 1140 C·km. Not all the observed sprites that were used for establishing the CMC-brightness relation were also used for the dimensional analysis, due to technical problems in establishing the star-field and computing the range to the sprite. This is reflected in the different numbers of data points in the respective graphs.

Figure 9 clearly shows that there is a positive correlation (R^2=0.7078) between the parent-lightning's charge moment change values and the radiance of sprites. Errors in the correlation are possibly due to uncertainty in the charge moment change values following ELF timing uncertainties or due to the inadequacy of the assumption on the current relaxation time in the CMC computation algorithm [Sato and Fukunishi, 2003]. As evident in Figure 9, similar CMC values may produce different sprite radiances. This could be explained by different combinations of the height-charge product which gives the CMC value (e.g a CMC value of 1000 [C·km] can be obtained by a lightning discharge of 250C at a height of 4 km, 200 C at 5 km or 166 C at 6 km). Clearly if the amount of charge lowered is smaller, then one would expect the induced QE-field to be smaller and so the sprite brightness would be smaller, too. In general we can conclude that higher CMC values result in brighter sprites, indicating that the charge moments play a major role in determining the sprite's luminosity, as was found by Takahashi et al. [2010] for column sprites.

The electric field imposed by the lightning, that ultimately drives the current in the sprite, is proportional to the charge moment change [Pasko et al., 1995]. Since the lightning charge transfer in the troposphere places a field on the mesosphere, we can surmise that the higher the charge lowered by the lightning is, the stronger the E field is, the higher the current in the sprite and the brighter the emission will be, (e.g 100C charge

can cause a brightness of ~10^5 R in the 1st positive band of N_2, ~300C charge can cause a brightness up to 10^7 R in the $N_2$1P band) [Pasko et al 1995].

The dielectric relaxation time is a measure of the time it takes for charge to become neutralized by conduction processes, and at mesospheric altitudes it is on order of a few milliseconds. Indeed, as evident from Figure 11, a significant positive correlation (~0.83) exists between the CMC values of the parent lightning and the length of the column sprites. The length of a sprite will depend on the duration of the mesospheric electric field, since it will allow streamers to propagate downwards to lower altitudes. Thus, one can deduce that the induced mesospheric QE field persists longer for stronger flashes that are lowering significant amounts of charge to the ground, resulting in the appearance of longer sprite columns in regular-rate video images [Pasko et al 2001]. The results are is a good agreement with those reported by Adachi et al. [2004].

Figure 10 presents a scatter plot of the number of column sprites and their respective values of charge moment. The correlation is weak (R^2=0.15), and the results are in good agreement with Adachi et al [2004] that reported no correlation between the numbers of column elements in sprite events and the values of the charge moment change of their parent flash. Adachi et al (2004) assumed that the number of column sprites is related to the peak current and the EMP rather than to the CMC and the quasi-electriostatic field. The role of the QE field is to initiate the breakdown for the formation of sprites but the role of the EMP on the other hand is to heat the electrons of the neutral atmosphere in a larger area, enabling the formation a large number of columns. The mechanism that governs the number of elements in a sprite is not yet known, and may reflect other factors such as neutral density fluctuations or the presence of meteoritic dust at sprite initiation

altitudes ~85-90 km. This issue requires further study.

5. Conclusions

We presented a methodology for calibrating a commercial CCD video camera, of the model frequently used by sprite researchers for regular-speed optical campaigns. This enabled us to obtain sprite luminosities which were found to range from 1.0-4.0 MR. Sprites in winter thunderstorms are produced by +CGs with CMC values in the range 110-1140 C·km. For column sprites, typical of such storms, there exists a linear relationship between the value of the charge moment change and the luminosity of the sprites: stronger flashes produce brighter sprites, which persist for longer durations and achieve a greater vertical extent. As for the number of sprite columns, a weak correlation was found with the parent flash CMC value, suggesting that other factors play a role.

Acknowledgments

The ILAN sprite campaigns are dedicated to the memory of the first Israeli astronaut Col. Ilan Ramon, lost with his crew members on board the Space Shuttle Columbia in February 2003. This work was supported by the Research Authority of the Open University of Israel, and by the Israeli Science Foundation grant 117/09.

REFERENCES

Adachi T., Fukunishi H., Takahashi Y., and Sato M., Roles of the EMP and QE field in the generation of columniform sprites, *Geophys. Res. Lett.*, Vol. 31, L04107, 2004.

Barrington-Leigh C.P., Inan U.S., Identification of sprites and elves with intensitified video and broadband array photometry. *Jour. Geophys. Res. 106, 1741–1750, 2001*.

Boccippio, D. J., E. R. Williams, S. J. Heckman, W. A. Lyons, I. T. Baker and R . Boldi, Sprites ELF transients and positive ground strokes, Science, 269, 1088, 1995

Bór, J., Sátori, G. and Betz, H-D., Observation of TLEs in Central Europe from Hungary Supported by LINET, in: Norma B. Crosby, Tai-Yin Huang, Michael J. Rycroft, Coupling of Thunderstorms and Lightning Discharges to Near-Earth Space: *Proceedings of the Workshop Corte (France), 23-27 June 2008, AIP Conference Proceedings Volume 1118, pp. 73-83, ISBN: 978-0-7354-0657-5, ISSN: 0094-243X, doi:10.1063/1.3137716*, 2009.

Bór, J., Optically perceptible characteristics of sprites observed in Central Europe in 2007–2009. *Jour. Atmos. Sol. Terr. Phys.*, 92, 151-177 doi.org/10.1016/j.jastp.2012.10.008, 2013.

Burke, C. P., and D. L. Jones, On the polarity and continuing currents in unusually large lightning flashes deduced from ELF events, *J. Atmos. Terr. Phys*., 58, 531–540, 1996.

Cummer S. A, and W. A. Lyons, Implication of lightning charge moment changes for sprite initiation. *J. Geophys. Res. 110, A04304. doi:10.1029/2004JA010812*, 2005.

Cummer S. A, Jaugey N. C, Li J. B, Lyons W. A, Nelson T. E and Gerken E. A, Submillisecond imaging of sprite development and structure, *Geophys. Res. Lett*., 33 L04104, 2006.

Cummer, S. A., and U. S. Inan, Modeling ELF radio atmospheric propagation and extracting lightning currents from ELF observations, *Radio Sci*., 35(2), 385–394, 2000.

Devir A., Ben-Shalom A., Balfour L.S, Engel M., Levin S., Progress in Radiometry – Measurement Techniqus and Analysis Methods, *Proc. SPIE, Vol. 3061, 626. 1997*.

Ganot M., Yair Y.v, Price C.n, Ziv B., Sherez Y, Greenberg E., Devir D.A., and Yaniv R., , First detection of transient luminous events associated with winter thunderstorms in the eastern Mediterranean, *Geophys. Res. Lett,*. 34, L12801, 2007.

Greenberg E., Price C., Yair Y., Ganot M., Bor J. and Satori G., ELF transients associated with sprites and elves in eastern Mediterranean winter thunderstorms, *Jour. Atmos. Solar Terr. Phys*., 69, 13, 1569-1586, 2007.

Hampton D.L, Heavner M.J and Sentman D.D, Optical spectral characteristics of Sprites, *Geophys. Res. Lett*., 23, 89-93, 1996.

Hobara Y, Iwasaki N, Hayashida T, Tsuchiya N, Williams ER, Sera M, Ikegami Y and M. Hayakawa, New ELF observation site in Moshiri, Hokkaido, Japan and the results of preliminary data analysis. *J. Atm. Electr*. 20: 99–109, 2000.

Hobara Y, Iwasaki N, Hayashida T, Hayakawa M, Ohta K, and H. Fukunishi, Interrelation between ELF transients and ionospheric disturbances in association with sprites and elves. *Geophys. Res. Lett*. 28: 935–938, 2001.

Hu, W., S. A. Cummer, W. A. Lyons, and T. E. Nelson, Lightning charge moment changes for the initiation of sprites, *Geophys. Res. Lett*., 29 (8), 1279, doi:10.1029/2001GL014593, 2002.

Huang, E., E. Williams, R. Boldi, S. Heckman, W. Lyons, M. Taylor, T. Nelson, and C. Wong, Criteria for sprites and elves based on Schumann resonance observations, *Jour. Geophys. Rres.*, 104(D14), 16,943–16,964, 1999.

Lu, G., S. A. Cummer, R. J. Blakeslee, S. Weiss, and W. H. Beasley (2012), Lightning morphology and impulse charge moment change of high peak current negative strokes, *J. Geophys. Res*., 117, D04212, doi:10.1029/2011JD016890.

Lyons W. A., Stanley M.A., Meyer J.D., Nelson T.E., Rutledge S.A., Lang T., Cummer S.A., The meteorological and electrical structure of TLE-producing convective storms, in Lightning: Principles, Instruments and Applications, ed. by H. Betz, U. Schumann, P. Laroche, pp. 387–415, (Springer, Berlin, 2009).

Matsudo Y., Suzuki T., Hayakawa M., Yamashita K., Ando Y., Michimoto K., Korepano V., Characteristics of Japanese winter sprites and their parent lightning as estimated by VHF lightning and ELF transients *Jour. Atmos. Solar Terr. Phys*., 69, 12, 1431–1446, 2007.

Montanya J., van der Velde O., Romero D., March V., Sola G., Pineda N., Arrayas M., Trueba J.L., Reglero V., Soula S., High- speed intensified video recordings of sprites and elves over the western Mediterranean Sea during winter thunderstorms, *Jour. Geophys. Res.*, 115, A00E18, doi:10.1029/2009JA014508, 2010.

Pasko, V.P., U.S. Inan, Y.N. Taranenko and T.F. bell, Heating, ionization and upward discharges in the mesosphere due to intense quasi-electrostatic thundercloud fields. *Geophys. Res. Lett, 22, 265, 1995.*

Pasko V. P, Inan U. S and Bell T. F, Mesosphere-troposphere coupling due to sprites, *Geophys. Res. Lett.*, Vol. 28, No. 19, pages 3821-3824, 2001.

Pasko V. P, Red sprite discharges in the atmosphere at high altitude: the molecular physics and the similarity with laboratory discharges, *Plasma Sources Sci. Technol*. 16 S13–S29, 2007.

Pasko, V. P.; Yair, Y., and Kuo, C.-L. (2011). Lightning Related Transient Luminous Events at High Altitude in the Earth's Atmosphere: Phenomenology, Mechanisms and Effects. *Space Science Reviews*, pp. 1-42, 0038-6308, DOI: 10.1007/s11214-011-9813-9.

Price, C., E. Greenberg, Y. Yair, G. Satori, J. Bor, H. Fukunishi, M. Sato, P. L. Israelevich, M. Moalem, A. Devir, Z. Levin, J. H. Joseph, I. Mayo, B. Ziv and A. Sternlieb, 2004: Ground-based detection of TLE-producing intense lightning during the MEIDEX mission on board the space shuttle Columbia. *Geophys. Res. Lett*., 31, L20107, doi:10.1029/2004GL020711

Qin, J., S. Celestin, and V. P. Pasko , Minimum charge moment change in positive and negative cloud to ground lightning discharges producing sprites, *Geophys. Res. Lett., 39*, L22801, doi:10.1029/2012GL053951, 2012.

Sao-Sabbas, F.T., Sentman D.D., Wescott E.M., Pinto O., Jr., Mendes O., Jr., and Taylor M.J., Statistical analysis of space-time relationships between sprites and lightning. *J. Atmos. Solar Terr. Phys., 65, 525-535, doi:10.1016/S1364-6826(02)00326-7*, 2003.

Sato, M., and H. Fukunishi, Global sprite occurrence locations and rates derived from triangulation of transient Schumann resonance events, *Geophys. Res. Lett*., 30(16), 1859, doi:10.1029/2003GL017291,2003.

Sato, M., H. Fukunishi, M. Kikuchi, H. Yamagishi, and W. A. Lyons, Validation of sprite-inducing cloud-to-ground lightning based on ELF observations at Syowa station in Antarctica, *J. Atmos. Solar-Terr. Phys.*, 65, 607– 614, 2003.

Sa´tori, G., M. Rycroft, P. Bencze, F. Ma¨rcz, J. Bo´r, V. Barta, T. Nagy and K. Kova´cs, An overview of thunderstorm-related research on the atmospheric electric field, Schumann Resonances, sprites, and the ionosphere at Sopron, Hungary. Surv Geophys, 34:255–292, doi10.1007/s10712-013-9222-6, 2013.

Soula S., Van der Velde O., Montanyà J., Neubert T., Chanrion O., Ganot M. - Analysis of thunderstorm and lightning activity associated with sprites observed during the EuroSprite campaigns: Two case studies. *Atmos. Res*., 91, 514-528 (2009).

Stenbaek-Nielsen H. C., M. G. McHarg, T. Kanmae, D. D. Sentman, Observed emission rates in sprite streamer heads, *Geophys. Res. Lett*., 34, 2007.

Suzuki T., Hayakawa M., Michimoto K., Small winter Thunderstorm with sprites and strong positive discharge, *IEEJ Tramsactions on Fundamentals and materials, 131, 9, 723-728,* 2011.

Takahashi, Y., A. Yoshida, M. Sato, T. Adachi, S. Kondo, R. -R Hsu, H -T Su, A. B. Chen, S. B. Mende, H. U. Frey, and L.–C. Lee, Absolute optical energy of sprites and its relationship to charge moment of parent lightning discharge based on measurement by ISUAL/AP, *Jour. Geophys. Res*., 115, A00E55, doi:10.1029/2009JA014814, 2010.

Tong L., Hiraki Y., Nanbu K., Fukunishi H., Release of positive charges producing sprite halos. *J. Atmos. Solar Terr. Phys.*, 67, 829–838, 2005.

Williams E., Valente M., Gerken E. and Golka R., Calibrated Radiance Measurements with an Air-Filled Glow Discharge Tube: Application to Sprites in the Mesosphere, M. Fullekrug et al. (eds.), Sprites, Elves and Intense Lightning Discharges, 237–251, Springer, 2006.

Williams ER, Lyons WA, Hobara Y, Mushtak VC, Asencio N, Boldi R, Bo´ r J, Cummer SA, Greenberg E, Hayakawa M, Holzworth RH, Kotroni V, Li J, Morales C, Nelson TE, Price C, Russell B, Sato M, Sa´tori G, Shirahata K, Takahashi Y, Yamashita K., Ground-based detection of sprites and their parent lightning flashes over Africa during the 2006 AMMA campaign. *Q J R Meteorol Soc*., 136, 257-271, doi:10.1002/qj.489, 2010.

Yair, Y., C. Price, Z. Levin, J. Joseph, P. Israelevitch, A. Devir, M. Moalem, B. Ziv and M. Asfur, Sprite observations from the space shuttle during the Mediterranean Israeli Dust Experiment (MEIDEX). *J. Atmos. Sol. Terr. Phys.*, 65, 635-642, 2003.

Yair Y., Israelevich P., Devir A.D., Moalem M., Price C., Joseph J.H., Levin Z., Ziv B., Sternlieb A., and A. Teller, New observations of sprites from the space shuttle, *Jour. Geophys. Res.*, D15, D15201/10.1029/2003JD004497, 2004.

Yair, Y., et al., Optical observations of transient luminous events associated with winter thunderstorms near the coast of Israel. *Atmos. Res.*, 91(2-4): p. 529-537,2009.

Yair, Y., R. Aviv and G. Ravid, Clustering and synchronization of lightning flashes in adjacent thunderstorm cells from lightning location networks data, *J. Geophys. Res.*, 114, D09210, doi:10.1029/2008JD010738, 2009.

Yaniv R., Devir A., Yair Y., Price C., Ziv B. and Reicher N., Calibration of CCD cameras for measurements of sprites and elves, *Proceedings of the Workshop Corte*

(France), 23-27 June 2008, AIP Conference Proceedings Volume 1118, pp. 73-83, ISBN: 978-0-7354-0657-5, ISSN: 0094-243X, doi:10.1063/1.3137716. (2009).

Figure Captions

Figure 1: An IR satellite image from December 11th, 2009 at 0130 UT. A deep Cyprus low is situated over Crete as it moves eastward. Lightning locations are denoted by red points, based on the WWLLN data. A total of 37 sprites (columns, carrots, angels) were imaged during a 5 hour period.

Figure 2: The filter transmittance shown with the quantum efficiency of the camera, the atmospheric transmittance and a typical spectrum of a red sprite.

Figure 3: K' curve in a GL vs. radiance [R] graph of the calibration source.

Figure 4: (a) The background ROI on the right side and (b) its histogram. (c) the background ROI on the left side and (d) its histogram. (e) the ROI of the sprite and its surrounding and (f) its histogram.

Figure 5: The GL histogram of the backgrounds and sprite ROIs

Figure 6: The horizontal cut (left). Horizontal plot (right).

Figure 7: TLE frame (left), frame before TLE (middle), subtraction result (right).

Figure 8: The vertical cut (left). Vertical plot (right).

Figure 9: The radiance of sprites versus charge moment change

Figure 10: the number of sprite column elements as a function of the charge moment change.

Figure 11: The average length of sprite column in a sprite event, as a function of the charge moment change.

Figure 1:

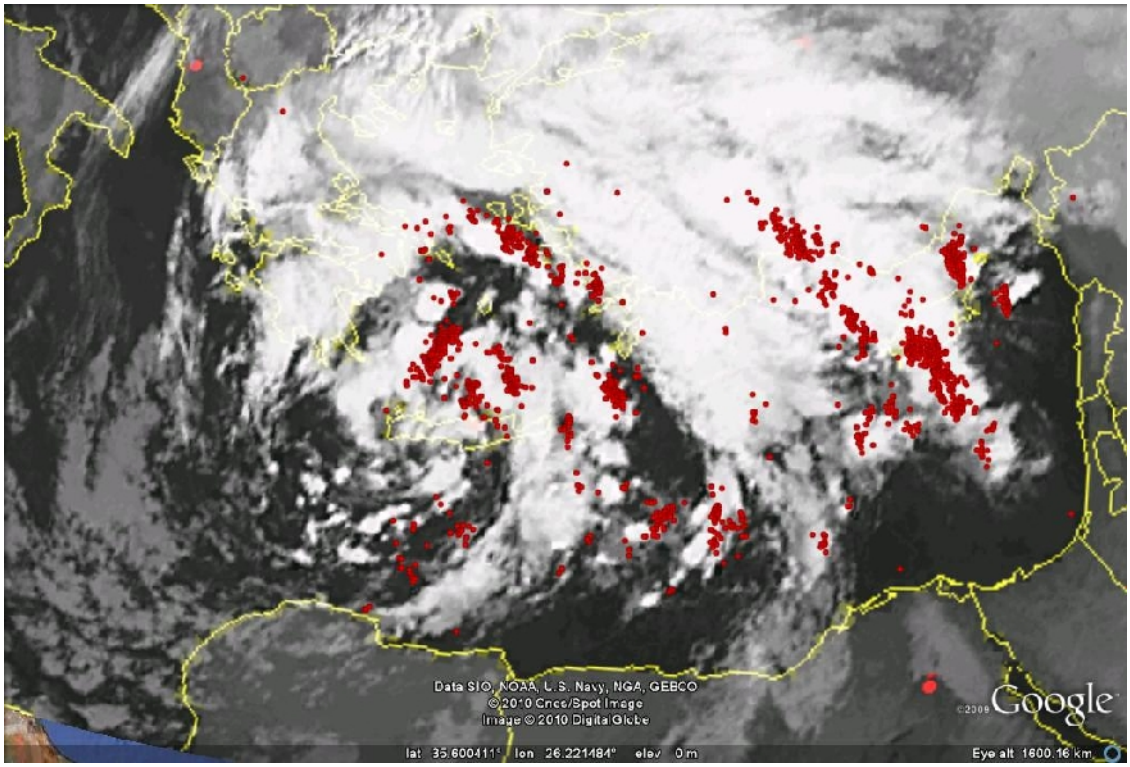

Figure 2:

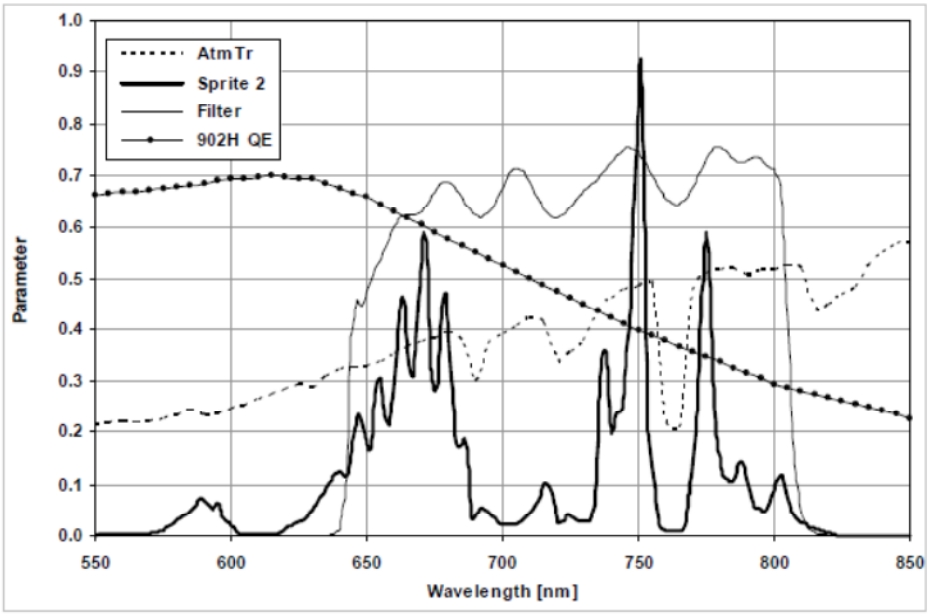

Figure 3:

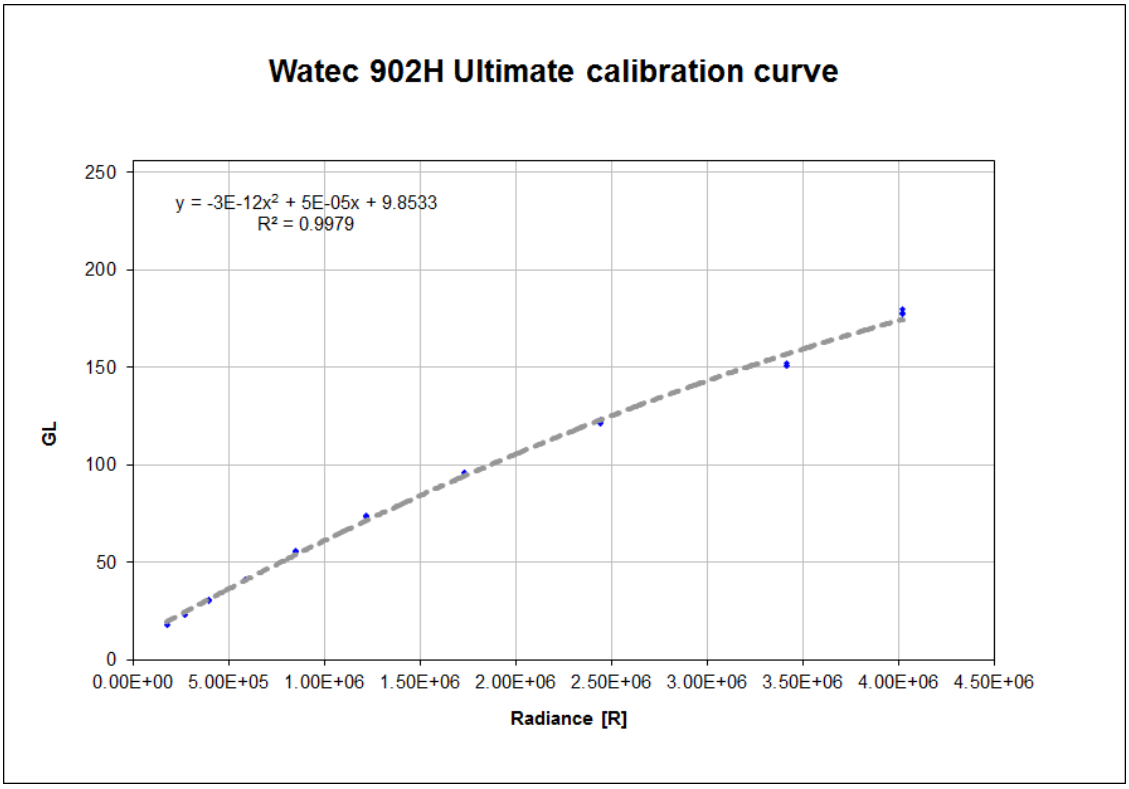
Watec 902H Ultimate calibration curve
y = -3E-12x² + 5E-05x + 9.8533
R² = 0.9979
GL
250
200
150
100
50
0
0.00E+00
5.00E+05
1.00E+06
1.50E+06
2.00E+06
2.50E+06
3.00E+06
3.50E+06
4.00E+06
4.50E+06
Radiance [R]

Figure 4:

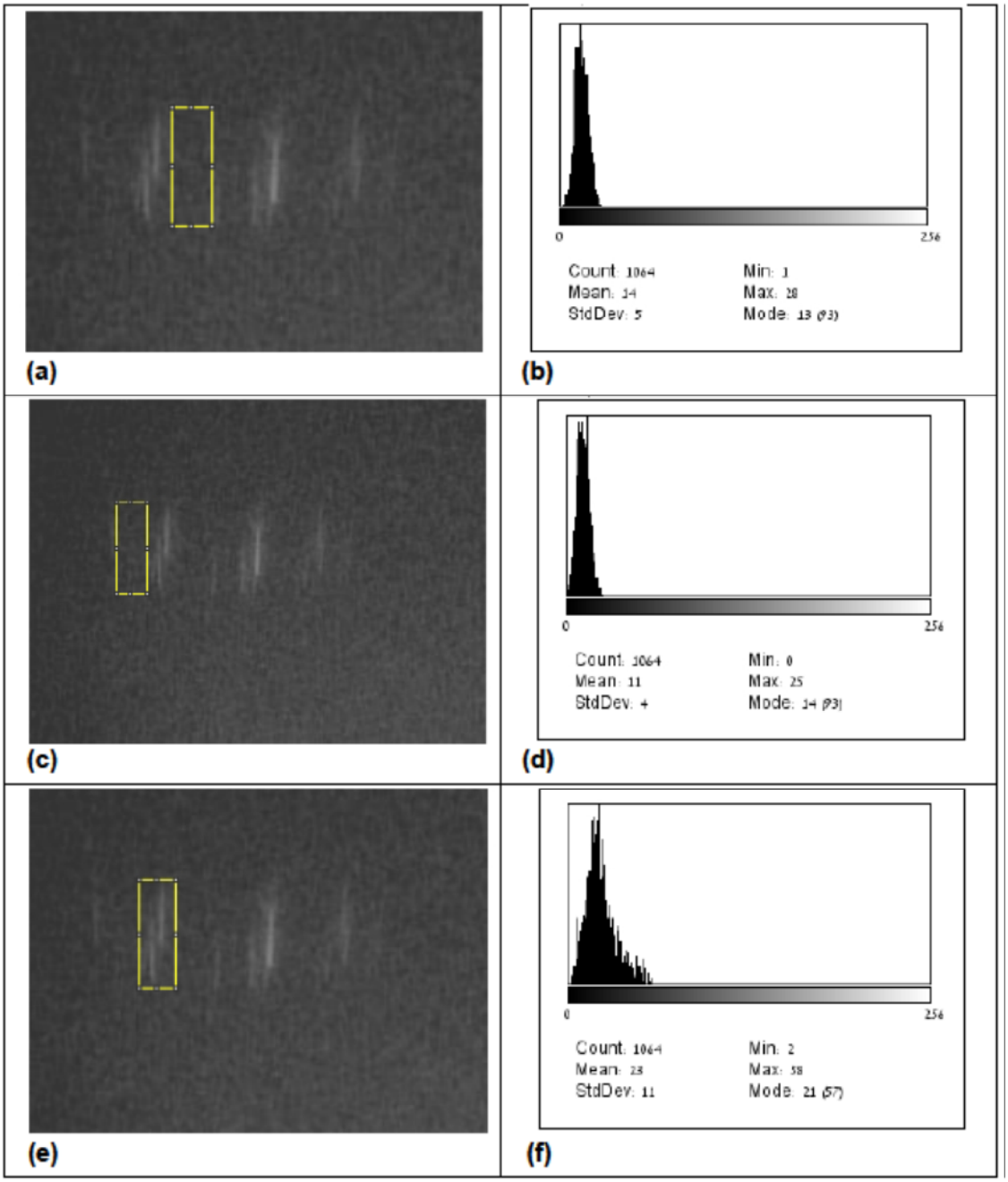
(a)
(b)
0
256
Count: 1064
Mean: 14
StdDev: 5
Min: 1
Max: 28
Mode: 13 (93)
(c)
(d)
0
256
Count: 1064
Mean: 11
StdDev: 4
Min: 0
Max: 25
Mode: 14 (93)
(e)
(f)
0
256
Count: 1064
Mean: 23
StdDev: 11
Min: 2
Max: 58
Mode: 21 (57)

Figure 5:

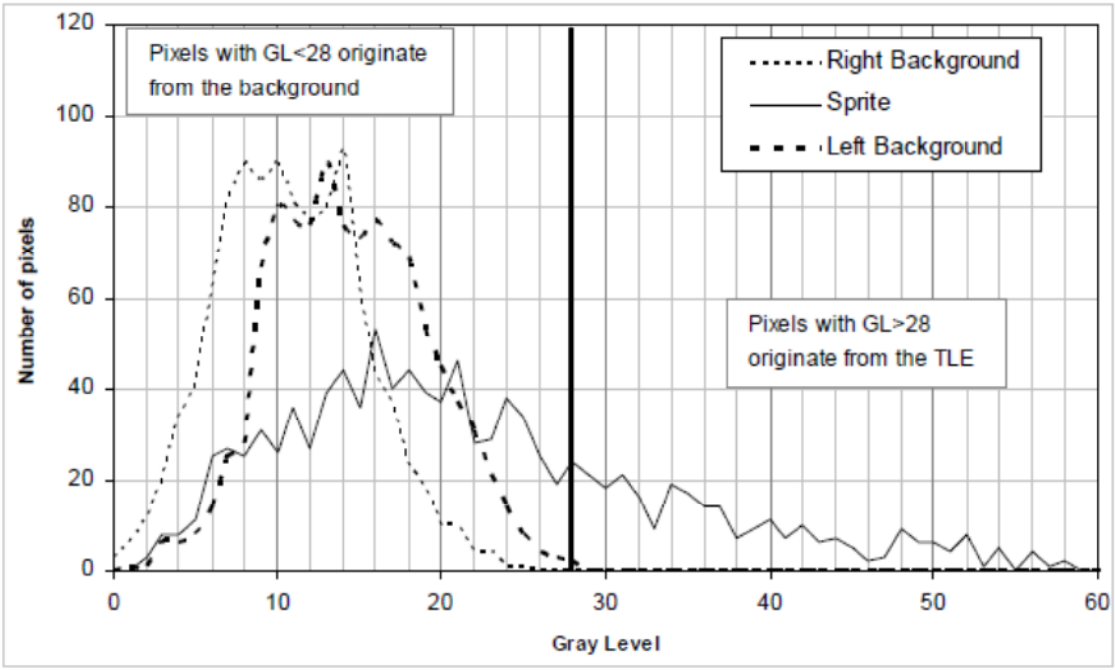

Figure 6:

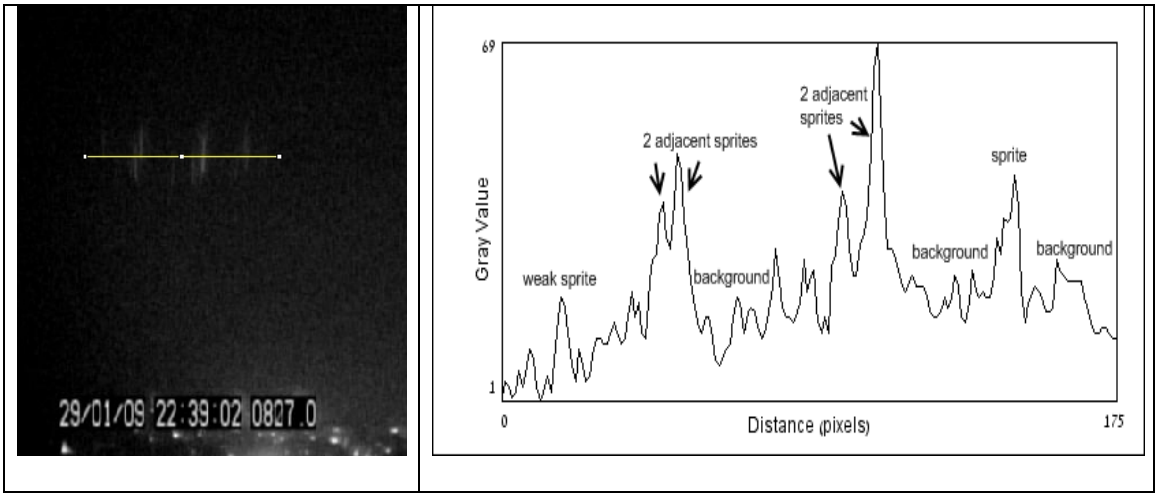

Figure 7:

Figure 8:

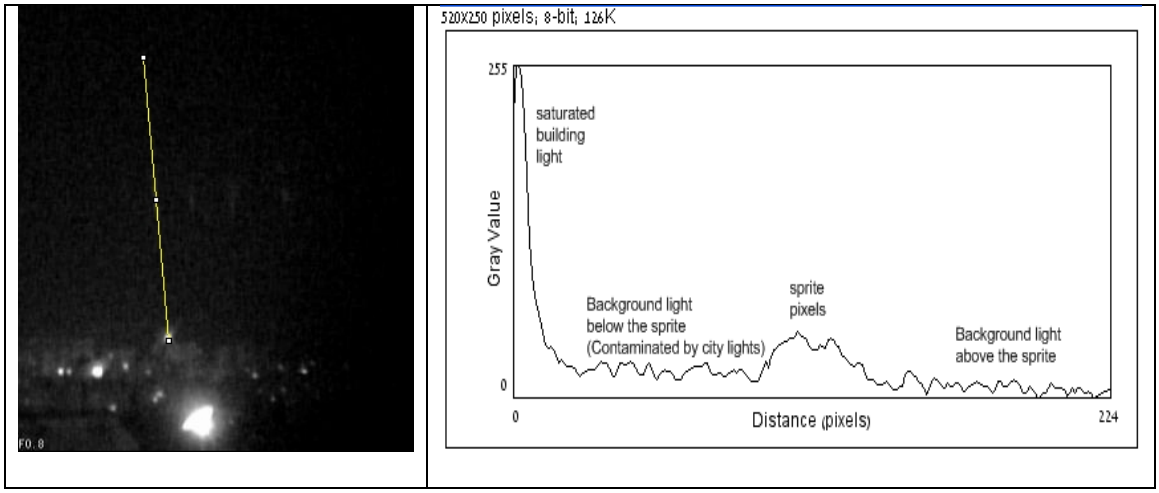

Figure 9:

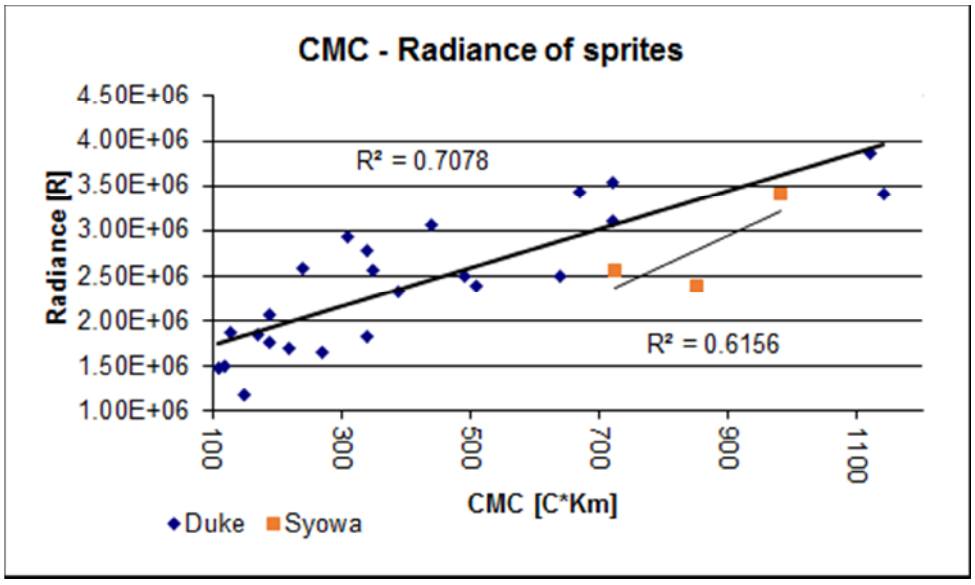

Figure 10:

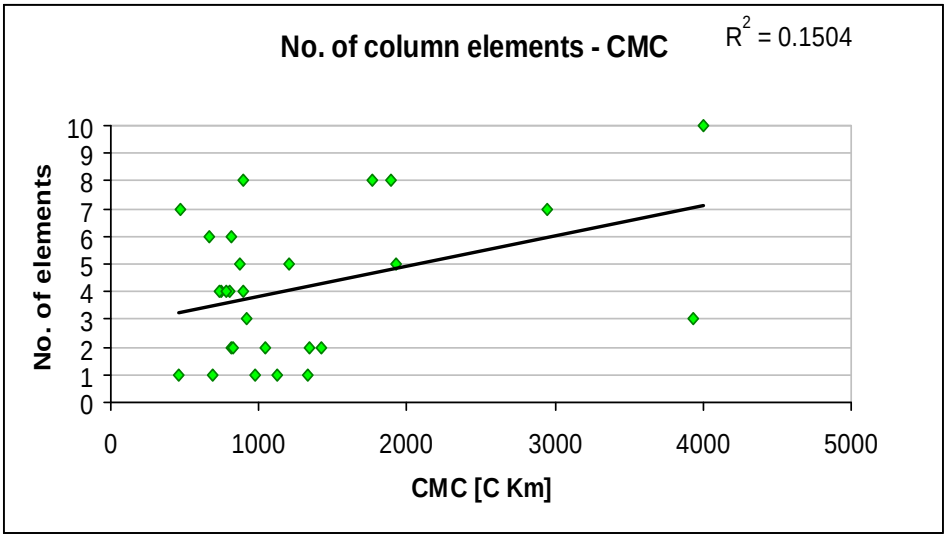

Figure 11: